

Electrostatic shielding effect and Binding energy shift of MoS₂, MoSe₂ and MoTe₂ materials

Yaorui Tan, Maolin Bo*

Key Laboratory of Extraordinary Bond Engineering and Advanced Materials Technology (EBEAM) of Chongqing, Yangtze Normal University, Chongqing 408100, China

*Corresponding Author: E-mail: bmlwd@yznu.edu.cn (Maolin Bo)

Abstract

In this paper, the electronic structure and bond properties of MoS₂, MoSe₂ and MoTe₂ are studied. Density functional theory (DFT) calculates combined with the binding energy and bond-charge (BBC) model to obtain electronic structure, binding energy shift and bond properties. It is found that electrostatic shielding by electron exchange is the main cause of density fluctuation. A method for calculating the density of Green's function with energy level shift is established. It provides new methods and ideas for the further study of the binding energy, bond states and electronic properties of nanomaterials.

Keywords: Electrostatic shielding effect, Binding energy shift, X-ray photoelectron spectroscopy, Density functional theory

1. Introduction

In the last two decades, two-dimensional(2D) layered of transition metal dihalides (TMDs) van der Waals materials, typical TMDs including MoS₂¹⁻⁵, MoSe₂^{6, 7 8}, and MoTe₂⁹⁻¹¹ materials, have made breakthrough developments in the light-emitting diodes, and photodetection and other optical devices. For example, the different phase 2D structures of MoS₂, combined with its large specific surface area advantage, are often used as catalysts or carriers in traditional multiphase thermal catalysis, photocatalysis and electrocatalysis. MoS₂ nanosheets as catalysts for Hydrogen evolution reaction¹². For MoSe₂, its optical band gap range is between 1.2-1.3 eV. This means that MoSe₂ can absorb visible and near-infrared light, making it widely used in the fields of Field-effect transistors¹³ and optoelectronics. For MoTe₂, it is a typical topological quantum material^{14, 15} of the MX₂ family of layered transition metal chalcogenides. Therefore, TMDs materials have been extensively studied and reported recently.

X-ray photoelectron spectroscopy (XPS) is a very powerful tool for studying the surface properties of materials. Researchers can obtain the binding energy (BE) of materials by photoelectron spectroscopy measurement. The BE of the same element in different compounds is different, and there is a phenomenon of energy shift. However, the energy shift is related to the electronic structure and bond properties of the material. Therefore, it is necessary to study electronic structure and bond properties of MoS₂, MoSe₂ and MoTe₂ through energy shifts.

In this paper, we calculated the electronic structure and bond properties of MoS₂, MoSe₂ and MoTe₂ using DFT calculates combined with the BBC model¹⁶. We found electrostatic shielding by electron exchange is the main cause of density fluctuation. Combined with the band theory and Green's function, the relationship between energy shift and lattice density is established, and the overlapping integral and three-dimensional bond-electron band are obtained by lattice density calculation. It provides new methods and ideas for the further study of the atomic bonding and electronic properties of nanomaterials.

2. Methods

2.1 DFT calculations

All the structural relaxation and electronic properties of MoS₂, MoSe₂ and MoTe₂ materials was investigated with the Cambridge Sequential Total Energy Package (CASTEP), which used total energy with a plane-wave pseudopotential. This analysis was focused on analyzing the atomic structure, energetics, and electronic properties of MoS₂, MoSe₂ and MoTe₂ materials. We used the Perdew–Burke–Ernzerhof (PBE)¹⁷ to describe the electron exchange and correlation potential. Additionally, in order to consider the long-range vdW interaction, we used TS scheme for DFT-D dispersion correction. The lattice parameters, cutoff energy and k -point grids, as shown in **Table 1 and 2**. The vacuum space was approximately 14 Å. In the calculations, all the atoms were completely relaxed such that the energy converged to 1×10^{-6} and the force on each atom converged to <0.01 eV/ Å.

2.2 BBC model

The BBC model is quantified chemical bonds by BE shift and deformation charge density. For the BE model, we use the central field approximation and Tight-binding model, which can get the relationship between the energy shift and Hamiltonian. For the bond-charge (BC) model, we use deformation charge density to calculate bonding states and electrostatic shielding by electron exchange is the main cause of density fluctuation.

For BE model:

$$\left\{ \begin{array}{l} H = \int \Psi^+(\vec{r})h(\vec{r})\Psi(\vec{r})d\vec{r} = \sum_{l,l'} C_l^+ C_{l'} \int a^*(\vec{r}-\vec{l})h(\vec{r})a(\vec{r}-l')d\vec{r} \\ H = \xi(0) \sum_l \hat{n}_l - t \sum_l \sum_\rho C_l^+ C_{l+\rho} \\ t = \sum_{l,l'} C_l^+ C_{l'} \int a^*(\vec{r}-\vec{l}) [V(\vec{r}) - v_a(\vec{r}-\vec{l})] a(\vec{r}-l') d\vec{r} \\ \sum_l \hat{n}_l = C_l^+ C_l \end{array} \right. \quad (1)$$

$V(r)$ is the potential and $v_a(\vec{r}-\vec{l})$ is the atomic potential, $\xi(0)$ is the local orbital electron energy. \hat{n}_l represents the electron number operator in the wanier representation.

$$\begin{cases}
\xi(0) = (E_n^a - A_n) \\
A_n = -\int a_n^*(\vec{r}-\vec{l}) [V(\vec{r}) - v_a(\vec{r}-\vec{l})] a_n(\vec{r}-\vec{l}) d\vec{r} \\
E_n^a = \int a_n^*(\vec{r}-\vec{l}) \left[-\frac{\hbar^2}{2m} \nabla^2 + v_a(\vec{r}-\vec{l}) \right] a_n(\vec{r}-\vec{l}) d\vec{r} \\
\Psi(\vec{r}) = \sum_l C_l a(\vec{r}-\vec{l})
\end{cases} \quad (2)$$

E_n^a is the atomic energy level and t is called the overlapping integral. A_n represents the energy shift E_n^a caused by the potential of $N-1$ atoms outside the lattice point l in the lattice.

Consider the effect of external fields on energy shifts:

$$\begin{cases}
H' = \xi(0) \sum_l \hat{n}_l - t \sum_l \sum_\rho C_l^+ C_{l+\rho} = (E_n^a - \gamma A_n) \sum_l \hat{n}_l - \gamma t \sum_l \sum_\rho C_l^+ C_{l+\rho} \\
\Delta E_v(B) = A_n \sum_l \hat{n}_l, \quad \Delta E_v(x) = \gamma A_n \sum_l \hat{n}_l \\
V_{cry}(\vec{r}_i - \vec{l}_j) = V(\vec{r}) - v_a(\vec{r} - \vec{l}) \\
\gamma V_{cry}(\vec{r}_i - \vec{l}_j) = \gamma \sum_{i,j,l_j \neq 0} \frac{1}{4\pi\epsilon_0} \frac{Z'e^2}{|\vec{r}_i - \vec{l}_j|} = \gamma \sum_{i,j,l_j \neq 0} \frac{1}{4\pi\epsilon_0} \frac{(Z - \lambda_v)e^2}{|\vec{r}_i - \vec{l}_j|} \\
\Delta E_v(x) = \gamma \int a_n^*(\vec{r}-\vec{l}) \sum_{i,j,l_j \neq 0} \frac{1}{4\pi\epsilon_0} \frac{(Z - \lambda_v)e^2}{|\vec{r}_i - \vec{l}_j|} a_n(\vec{r}-\vec{l}) d\vec{r} \sum_l \hat{n}_l \\
\Delta E_v(x) = \gamma \langle \Psi_v(\vec{r}) | \sum_{i,j,R_j \neq 0} \frac{1}{4\pi\epsilon_0} \frac{(Z - \lambda_v)e^2}{|\vec{r}_i - \vec{l}_j|} | \Psi_v(\vec{r}) \rangle
\end{cases} \quad (3)$$

The effective positive charge of the ion is $Z' = Z - \lambda_v$, considering the charge shielding effect λ_v , where Z is the nuclear charge. $\Delta E_v(B)$ is represents the energy shift of an atom in an ideal bulk. $\delta\gamma = \gamma - 1$ is relative BE ratio and B indicates bulk atoms.

The energy shifts in an external field obtained from **Eq. 3** are¹⁶:

$$\left\{ \begin{array}{l}
\delta\gamma = -1(\text{Antibonding}), \Delta E_v(x) = \Delta E_v(0) = 0 \quad (\text{isolated atom, neutral atom}) \\
\delta\gamma = 0(\text{Bonding}), \Delta E_v(x) = \Delta E_v(B) = -\left(-\sum_{l, R_l \neq 0} \langle \phi_v(r) | \frac{1}{4\pi\epsilon_0} \frac{Ze^2}{|\vec{r} - \vec{R}_l|} | \phi_v(r) \rangle\right) > 0 \quad (\text{bulk atoms, core level loses electrons}) \\
\delta\gamma > 0 \left\{ \begin{array}{l}
\delta\gamma > 1(\text{Bonding}), \Delta E_v(x) = -\left(-\langle \phi_v(r) | \sum_{l, R_l \neq 0} \frac{(1+\delta\gamma)}{4\pi\epsilon_0} \frac{Ze^2}{|\vec{r} - \vec{R}_l|} | \phi_v(r) \rangle\right) > 0 \quad (\text{potential well becomes deeper}) \\
1 > \delta\gamma > 0(\text{Bonding}), \Delta E_v(x) = -\left(-\langle \phi_v(r) | \sum_{l, R_l \neq 0} \frac{(1+\delta\gamma)}{4\pi\epsilon_0} \frac{Ze^2}{|\vec{r} - \vec{R}_l|} | \phi_v(r) \rangle\right) > 0 \quad (\text{core level loses electrons})
\end{array} \right. \\
\delta\gamma < 0 \left\{ \begin{array}{l}
-1 < \delta\gamma < 0(\text{Nonbonding}), \Delta E_v(x) = -\left(-\sum_{l, R_l \neq 0} \langle \phi_v(r) | \frac{(1+\delta\gamma)}{4\pi\epsilon_0} \frac{Ze^2}{|\vec{r} - \vec{R}_l|} | \phi_v(r) \rangle\right) > 0 \quad (\text{core level gets electrons}) \\
\delta\gamma < -1(\text{Antibonding}), \Delta E_v(x) = -\left(-\sum_{l, R_l \neq 0} \langle \phi_v(r) | \frac{(1+\delta\gamma)}{4\pi\epsilon_0} \frac{Ze^2}{|\vec{r} - \vec{R}_l|} | \phi_v(r) \rangle\right) < 0 \quad (\text{potential well becomes shallower or barrier potential})
\end{array} \right.
\end{array} \right. \quad (4)$$

Eq.4 was obtained by calculating the external field-induced BE ratio, γ , using the known reference values of $\Delta E'_v(x) = E_v(x) - E_v(B)$, $\Delta E_v(B) = E_v(B) - E_v(0)$, and $\Delta E_v(x) = E_v(x) - E_v(0)$ derived from XPS analysis. Then, we obtain

$$\gamma = \frac{E_v(x) - E_v(0)}{E_v(B) - E_v(0)} \approx \frac{Z_x}{Z_b} \frac{d_b}{d_x} = \left(\frac{Z_b - \lambda'_v}{Z_b} \right) \left(\frac{d_x}{d_b} \right)^{-1} = \left(\frac{d_x}{d_b} \right)^{-m} = \frac{E_x}{E_b}, \quad (5)$$

λ'_v is the relative charge shielding factor. m is an indicator for the bond nature of a specific material. The m is related to the charge shielding factor λ'_v ,

$$m = 1 - \frac{\ln \frac{Z_b - \lambda'_v}{Z_b}}{\ln \left(\frac{d_x}{d_b} \right)}.$$

For BC model, we consider the positive charge background (b) and the electron (e) as a system, and write their Hamiltonian sums and their interactions, respectively. In addition to electron kinetic energy, only electrostatic Coulomb interactions are considered:

$$\begin{cases}
H = H_b + H_e + H_{eb} \\
H_e = \sum_{i=1}^N \frac{P_i^2}{2m} + \frac{1}{2} e_1^2 \sum_{i=1}^N \sum_{\substack{j=1 \\ i \neq j}}^N \frac{1}{|r_i - r_j|} e^{-\lambda|r_i - r_j|} \\
H_b = \frac{1}{2} e_1^2 \int d^3x \int d^3x' \frac{n(x)n(x')}{|x - x'|} e^{-\lambda|x - x'|} = \frac{1}{2} e_1^2 \left(\frac{N}{V} \right)^2 \int d^3x 4\pi \int dz \frac{e^{-\lambda z}}{z} = 4\pi e_1^2 \frac{N^2}{2V\lambda^2} \\
H_{eb} = -e_1^2 \sum_{i=1}^N \int d^3x \frac{n(x)}{|x - r_i|} e^{-\lambda|x - r_i|} = -e_1^2 \sum_{i=1}^N \frac{N}{V} 4\pi \int dz \frac{e^{-\lambda z}}{z} = -4\pi e_1^2 \frac{N^2}{V\lambda^2}
\end{cases} \quad (6)$$

The shielding factor λ is added to the equation. r_i represents the i th electronic position.

x represents the background position. e is the basic charge, $e_1 = e/\sqrt{4\pi\epsilon_0}$. $e_1 n(x)$ is the charge density at background x , and $n(x) = N/V$ is a constant.

$$\begin{cases}
H_e = \sum_{i=1}^N \frac{P_i^2}{2m} + \frac{1}{2} e_1^2 \sum_{i=1}^N \sum_{\substack{j=1 \\ i \neq j}}^N \frac{1}{|r_i - r_j|} e^{-\lambda|r_i - r_j|} \\
= \sum_{k\sigma} \frac{\hbar^2 k^2}{2m} a_{k\sigma}^\dagger a_{k\sigma} + \frac{e_1^2}{2V} \sum_q^* \sum_{k\sigma} \sum_{k'\lambda} \frac{4\pi}{q^2 + \lambda^2} a_{k+q,\sigma}^\dagger a_{k'-q,\lambda}^\dagger a_{k'\lambda} a_{k\sigma} + \frac{e_1^2}{2V} \frac{4\pi}{\lambda^2} (N^2 - N) \\
\sum_{i=1}^N \frac{P_i^2}{2m} = \sum_{l'\sigma'} \sum_{l\sigma} a_{k_l\sigma'}^\dagger \left\langle k_l\sigma' \left| \frac{P^2}{2m} \right| k_l\sigma \right\rangle = \sum_{l\sigma} \frac{\hbar^2 k_l^2}{2m} a_{k_l\sigma}^\dagger a_{k_l\sigma} \\
\frac{1}{2} e_1^2 \sum_{i=1}^N \sum_{\substack{j=1 \\ i \neq j}}^N \frac{1}{|r_i - r_j|} e^{-\lambda|r_i - r_j|} = \frac{e_1^2}{2V} \sum_q \sum_{k'} \sum_{\sigma\lambda} \frac{4\pi}{q^2} a_{k+q,\sigma}^\dagger a_{k'-q,\lambda}^\dagger a_{k'\lambda} a_{k\sigma}
\end{cases} \quad (7)$$

In the formula, the q on the sum sign of "*" indicates that the part where $q = 0$ is ignored during the sum. When $V \rightarrow \infty, N \rightarrow \infty$, while keeping N/V constant, the last term to the right of the equal sign causes the average energy H_e/N of each particle to become:

$$\frac{1}{2} 4\pi e_1^2 \left(\frac{N}{V} \right) \frac{1}{\lambda^2} - \frac{1}{2} 4\pi e_1^2 \left(\frac{N}{V} \right) \frac{1}{N} \frac{1}{\lambda^2}$$

The former term is constant, and the latter term tends to zero. If $\lambda \rightarrow 0$, the former term becomes a divergent term. However, this term just cancels out the divergent H_b

and H_{eb} term. Thus, the Hamiltonian of the system becomes:

$$H = \sum_{k\sigma} \frac{\hbar^2 k^2}{2m} a_{k\sigma}^\dagger a_{k\sigma} + \frac{e_1^2}{2V} \sum_q \sum_{k'} \sum_{\sigma\lambda} \frac{4\pi}{q^2} a_{k+q,\sigma}^\dagger a_{k'-q,\lambda}^\dagger a_{k'\lambda} a_{k\sigma} \quad (8)$$

Electron interactions expressed using electron density:

$$\left\{ \begin{aligned} \hat{V}_{ee} &= \frac{e_1^2}{2V} \sum_k \sum_{k'} \sum_{\sigma\lambda} \frac{4\pi}{q^2} a_{k+q,\sigma}^\dagger a_{k'-q,\lambda}^\dagger a_{k'\lambda} a_{k\sigma} = \frac{1}{2} \sum_{k_1 k_2, k_1' k_2'} \sum_{\sigma_1 \sigma_2} \langle k_1, k_2 | v | k_1', k_2' \rangle C_{k_1 \sigma_1}^+ C_{k_2 \sigma_2}^+ C_{k_2' \sigma_2} C_{k_1' \sigma_1} \\ &= \frac{1}{4\pi\epsilon_0} \times \frac{1}{2|\vec{r} - \vec{r}'|} \int d^3 r \int d^3 r' \rho(\vec{r}) \rho(\vec{r}') \\ V'_{ee} &= \frac{e_1^2}{2V} \sum_k \sum_{k'} \sum_{\bar{q}} \sum_{\sigma\lambda} \frac{4\pi}{q^2 + \lambda^2} a_{\vec{k} + \bar{q}, \sigma}^+ a_{\vec{k}' - \bar{q}, \lambda}^+ a_{\vec{k}' \lambda} a_{\vec{k} \sigma} = \frac{1}{4\pi\epsilon_0} \frac{1}{2|\vec{r} - \vec{r}'|} \int d^3 r \int d^3 r' \rho(\vec{r}) \rho(\vec{r}') e^{-\lambda(\vec{r} - \vec{r}')} \\ \rho(\vec{r}) &= a_{k+q,\sigma}^\dagger a_{k\sigma} = C_{k_1 \sigma_1}^+ \psi_{k_1}^*(r) C_{k_1 \sigma_1} \psi_{k_1}(r) \\ \langle k_1, k_2 | v | k_1', k_2' \rangle &= \int \frac{e^2 \psi_{k_1}^*(r) \psi_{k_2}^*(r') \psi_{k_1}(r) \psi_{k_2}(r')}{4\pi\epsilon_0 |r - r'|} dr dr' \end{aligned} \right. \quad (9)$$

Electron interaction terms for density fluctuations:

$$\left\{ \begin{aligned} \delta V_{ee} &= V'_{ee} - V_{ee} \\ &= \frac{1}{4\pi\epsilon_0} \frac{1}{2|\vec{r} - \vec{r}'|} \int d^3 r \int d^3 r' \delta\rho(\vec{r}) \delta\rho(\vec{r}') \\ &= \frac{1}{4\pi\epsilon_0} \frac{1}{2|\vec{r} - \vec{r}'|} \int d^3 r \int d^3 r' \rho(\vec{r}) \rho(\vec{r}') (e^{-\lambda(\vec{r} - \vec{r}')} - 1) \\ &= \frac{1}{4\pi\epsilon_0} \frac{1}{2|\vec{r} - \vec{r}'|} \int d^3 r \int d^3 r' \delta'\rho(\vec{r}) \delta'\rho(\vec{r}') - \frac{1}{4\pi\epsilon_0} \frac{1}{2|\vec{r} - \vec{r}'|} \int d^3 r \int d^3 r' \rho(\vec{r}) \rho(\vec{r}') \\ &= \frac{e_1^2}{2V} \sum_k \sum_{k'} \sum_{\bar{q}} \sum_{\sigma\lambda} \frac{4\pi}{q^2 + \mu^2} a_{\vec{k} + \bar{q}, \sigma}^\dagger a_{\vec{k}' - \bar{q}, \lambda}^\dagger a_{\vec{k}' \lambda} a_{\vec{k} \sigma} - \frac{e_1^2}{2V} \sum_k \sum_{k'} \sum_{\sigma\lambda} \frac{4\pi}{q^2} a_{k+q,\sigma}^\dagger a_{k'-q,\lambda}^\dagger a_{k'\lambda} a_{k\sigma} \\ \delta V_{bc} &= \delta V_{ee} = \frac{1}{4\pi\epsilon_0} \frac{1}{2|\vec{r} - \vec{r}'|} \int d^3 r \int d^3 r' \delta\rho(\vec{r}) \delta\rho(\vec{r}') \end{aligned} \right. \quad (10)$$

Also, $\delta\rho$ satisfies the following relationship¹⁶:

$$\left(\delta\rho_{\text{Hole-electron}} \leq \delta\rho_{\text{Antibonding-electron}} < \delta\rho_{\text{No charge transfer}} = 0 < \delta\rho_{\text{Nonbonding-electron}} \leq \delta\rho_{\text{Bonding-electron}} \right) \quad (11)$$

For atomic (strong) bonding states:

$$\delta\rho_{\text{Hole-electron}}(\vec{r})\delta\rho_{\text{Bonding-electron}}(\vec{r}') < 0 \text{ (Strong Bonding)}. \quad (12)$$

For atomic nonbonding or weak-bonding states:

$$\left\{ \begin{array}{l} \delta\rho_{\text{Hole-electron}}(\vec{r})\delta\rho_{\text{Nonbonding-electron}}(\vec{r}') < 0 \text{ (Nonbonding or Weak Bonding)} \\ \delta\rho_{\text{Antibonding-electron}}(\vec{r})\delta\rho_{\text{Bonding-electron}}(\vec{r}') < 0 \text{ (Nonbonding or Weak Bonding)} \\ \delta\rho_{\text{Antibonding-electron}}(\vec{r})\delta\rho_{\text{Nonbonding-electron}}(\vec{r}') < 0 \text{ (Nonbonding)} \end{array} \right. \quad (13)$$

For atomic antibonding states:

$$\left\{ \begin{array}{l} \delta\rho_{\text{Nonbonding-electron}}(\vec{r})\delta\rho_{\text{Bonding-electron}}(\vec{r}') > 0 \text{ (Antibonding)} \\ \delta\rho_{\text{Hole-electron}}(\vec{r})\delta\rho_{\text{Antibonding-electron}}(\vec{r}') > 0 \text{ (Antibonding)} \\ \delta\rho_{\text{Hole-electron}}(\vec{r})\delta\rho_{\text{Hole-electron}}(\vec{r}') > 0 \text{ (Antibonding)} \\ \delta\rho_{\text{Antibonding-electron}}(\vec{r})\delta\rho_{\text{Antibonding-electron}}(\vec{r}') > 0 \text{ (Antibonding)} \\ \delta\rho_{\text{Nonbonding-electron}}(\vec{r})\delta\rho_{\text{Nonbonding-electron}}(\vec{r}') > 0 \text{ (Antibonding)} \\ \delta\rho_{\text{Bonding-electron}}(\vec{r})\delta\rho_{\text{Bonding-electron}}(\vec{r}') > 0 \text{ (Antibonding)} \end{array} \right. \quad (14)$$

The formation of bonds is related to fluctuations in electron density $\delta\rho$.

Hartree–Fock ground state energy formula:

$$\begin{aligned} \frac{E_0}{N} &= \frac{3}{5} \frac{\hbar^2 k_F^2}{2m} - \frac{3e^2}{4\pi} k_F + \frac{e^2}{2a_H} \varepsilon_c(r_s) \\ &= \frac{e^2}{2a_H} \left(\frac{2.21}{r_s^2} + \varepsilon_x(r_s) + \varepsilon_c(r_s) \right) \end{aligned} \quad (15)$$

Exchange correlation energy $\varepsilon_{xc}(r_s)$ ^{18,19}:

$$\begin{cases} \varepsilon_{xc}(r_s) = \varepsilon_x(r_s) + \varepsilon_c(r_s) \\ \varepsilon_c(r_s) = \begin{cases} -0.2846 / (1 + 1.0529\sqrt{r_s} + 0.3334r_s) & (r_s \geq 1) \\ -0.0960 + 0.0622 \ln r_s - 0.0232r_s + 0.0040r_s \ln r_s & (r_s \leq 1) \end{cases} \\ \varepsilon_x(r_s) = -0.9164 / r_s \end{cases} \quad (16)$$

$\varepsilon_c(r_s)$ represents the correlation energy and $\varepsilon_x(r_s)$ represents exchange energy.

3. Results and discussion

3.1 Geometric structure, density of states (DOS), band structure and deformation charge density

The geometric structure of the MoS₂, MoSe₂ and MoTe₂ are illustrated in **Fig. 1**. The optimized the lattice parameters are listed in **the Table 1**. For MoS₂, the lattice parameters in a , b , and c are 6.385, 6.385, and 6.385 Å, respectively. The lattice parameters in α , β and γ angle are $\alpha = 90.00^\circ$, $\beta = 90.00$, and $\gamma = 120.00^\circ$. In **Fig. 2**, the DOS of MoS₂, MoSe₂ and MoTe₂ were given. In the conductive band, the main peaks of the electron density distribution occur at -2.06 eV, -1.83 eV, and -1.46 eV for MoS₂, MoSe₂ and MoTe₂, respectively. The partial DOS of s and p , and d orbitals were analyzed for MoS₂, MoSe₂ and MoTe₂. The d orbitals contribute the vast majority of electrons in the valence and conduction bands.

We calculated the band structure of MoS₂, MoSe₂ and MoTe₂, as is shown in **Fig. 2**. The band gap values of MoS₂, MoSe₂ and MoTe₂ structures are 1.374 eV, 1.426 eV, and 1.016 eV, respectively. The semiconductors of MoS₂, MoSe₂ and MoTe₂ structures are all indirect bandgap semiconductor materials. MoS₂, MoSe₂ and MoTe₂ structures have optical bandgap ranges from 1.0 -1.5 eV range is adjustable, which means that visible and near-infrared light can be absorbed. **Fig. 3** exhibits the deformation charge density obtained by analyzing the calculated results of the MoS₂, MoSe₂ and MoTe₂ structures. For MoS₂, MoSe₂ and MoTe₂ structures, the information of electron distribution was provided by color scale. The blue and red areas represent the increase and decrease of the electron distribution respectively. The electrons in the positive region are convergent, while they are divergent in the negative region. The blue regions represent numerous electrons gathering, and the deformation charge density is positive. The red

regions represent numerous electrons divergent, and the deformation charge density is negative.

The established BBC model was used to convert the value of Hamiltonian into the value of bonding (**Table 3**). Using the **Eq. 10**, the deformation bond energy are -0.4851 eV, -1.2864 eV, and -0.7692 eV for MoS₂, MoSe₂ and MoTe₂, respectively. To develop a method that would enable the accurate analysis of the chemical bonding and the electronic properties of semiconductor materials.

3.2 Lattice density and bond properties

The lattice density formula for a three-dimensional lattice²⁰:

$$\rho_0(E) = \frac{2\theta(b - |E - \varepsilon_0|)}{\pi b^2} \sqrt{b^2 - (E - \varepsilon_0)^2} \quad (17)$$

When $|E - \varepsilon_0| < b$, there is $\theta(b - |E - \varepsilon_0|) = 1$. Considering the core energy level $E =$

$E_v(x)$, we can obtain:

$$\rho_0(E) = \frac{2}{\pi b^2} \sqrt{b^2 - (E_v(x) - E_v(I))^2} \quad (18)$$

Through the measurement of XPS experiment, we can obtain the BE of the electron and calculate the BE ratio. b is the Full width at half maximum (FWHM). The FWHM, BE and BE ratio of Mo, MoS₂, MoSe₂ and MoTe₂ are shown in **Table 4**. **Fig. 4** shows the lattice density of the BE of electrons at different core levels calculated by **Eq. 18**. Therefore, as long as we know the BE and FWHM, we can obtain the distribution of the lattice density of the core level.

The BE ratio is used as the input for the calculation of bond properties. By combining BOLS theory²¹ with the BBC model, we can further obtain²²:

$$\left\{ \begin{array}{ll}
E_v(I) = E_v(0) + \Delta E_v(B) \gamma^m & \text{(binding energy shift)} \\
\varepsilon_x = \gamma^{-1} - 1 & \text{(local bond strain)} \\
\delta E_C = z_x E_x / z_b E_b - 1 = z_{xb} \gamma^m - 1 & \text{(atomic cohesive energy)} \\
\delta E_D = (E_x / d_x^3) / (E_b / d_b^3) - 1 = \gamma^{m+3} - 1 & \text{(bond energy density)} \\
z_x = \frac{12}{\{8 \ln(2\gamma - 1) + 1\}} & \text{(atomic coordination number)} \\
t = b / z_x & \text{(overlapping integral)}
\end{array} \right. \quad (19)$$

For the bulk Mo atom energy level shift is $\Delta E_v(B) = 2.707$ eV, the single atom energy level shift is $E_v(0) = 224.862$ eV²³. For single metal materials, $m = 1$, while for compounds, there will be different bond nature indicator m . Using **Eq. 19**, we calculated local bond strain ε_x (%), relative atomic cohesive energy δE_C (%), relative bond energy density δE_D (%), BE ratio γ , coordination number (CN) z_x , FWHM b of Mo, MoS₂, MoSe₂ and MoTe₂.

From **Fig. 5**, we can see that the BE and atomic cohesive energy and bond energy density are related to the BE ratio. BE ratio γ is constant, the higher the m value is, the greater the BE and bond energy density are. The atomic cohesive energy of MoS₂, MoSe₂ and MoTe₂ is larger than that of the elemental element Mo. Our calculations provide a theoretical reference for the bonding properties of MoS₂, MoSe₂ and MoTe₂ semiconductor materials.

3.3 Energy scaling and electrostatic shielding

A static external disturbance corresponds to a frequency of $\omega = 0$, and the Thomas–Fermi dielectric function is as follows^{24, 25}:

$$\varepsilon_1(q, 0) \approx 1 + \left(\frac{6\pi N e^2}{E_F} \right) \frac{1}{q^2} \equiv 1 + \frac{\lambda^2}{q^2}, \quad (20)$$

where N is the number of lattice points, E_F is the Fermi energy, q is the wave vector. Using this formula to investigate the case in which there is a negative charge at the origin, the following Thomas–Fermi formula for the total potential energy can be

obtained:

$$V_{TF}(r) = \sum_q \frac{4\pi e^2}{q^2 + \lambda^2} e^{iqr} = \frac{e^2}{r} e^{-\lambda r}, \quad (21)$$

where V_{TF} is the electrostatic shielding potential. This equation demonstrates that a $(-e)$ charge located at the origin will be shielded within a distance of λ^{-1} , and the shielding effect of the electronic system will give rise to a Coulomb interaction between the electrons in the metal of e^2/r being converted into a Yukawa type interaction. The effect is then represented by $(e^2/r)\exp(-\lambda r)$, where λ and q_c are of the same magnitude, and q_c is the upper limit of the plasmon wavenumber. Here, we use electrostatic shielding to define the energy scaling factor L .

Considering the energy scaling factor L for the potential energy function, we can obtain the following:

$$L = \frac{|V_i(\vec{r}_{ij})|}{|V_0(\vec{r}_{ij})|} = e^{-\lambda_A r_{ij}}. \quad (22)$$

Next, we derive the following:

$$V_i(\vec{r}_{ij}) = V_0(\vec{r}_{ij}) e^{-\lambda_A r_{ij}} \quad (23)$$

$$V_i'(\vec{r}_{ij}) = -V_0(\vec{r}_{ij}) e^{-\lambda_B r_{ij}} \quad (24)$$

The electrostatic shielding parameter λ_A in **Eq. 23** is related to the electrostatic shielding effect. The value of λ_A is inversely proportional to this effect; therefore, the electronic polarization decreases as electrostatic shielding parameter λ_A increases, and the potential energy decreases. The electrostatic shielding parameter λ_B in **Eq. 24** is related to the antibonding potential energy. An increase in λ_B will simultaneously

decrease the antibonding potential energy.

According to **Eq.22**, further, we can obtain bonding potential energy ($\delta V_{bc} < 0$) and exchange correlation energy the following relationship:

$$(13.6\varepsilon_c(r_s) + \delta V_{bc}) = 13.6\varepsilon_c(r_s) e^{-\lambda_{A1} r_{ij}} \quad (25)$$

$$(13.6\varepsilon_c(r_s) + \delta V_{bc}) = \delta V_{bc} e^{-\lambda_{A2} r_{ij}} \quad (26)$$

$$t = -\delta V_{bc} e^{-\lambda_{A3} r_{ij}} \quad (27)$$

Then, we have antibonding potential energy ($\delta V_{bc} > 0$) and exchange correlation energy the following relationship:

$$|(13.6\varepsilon_c(r_s) + \delta V_{bc})| = |13.6\varepsilon_c(r_s)| e^{-\lambda_{B1} r_{ij}} \quad (28)$$

$$|(13.6\varepsilon_c(r_s) + \delta V_{bc})| = \delta V_{bc} e^{-\lambda_{B2} r_{ij}} \quad (29)$$

$$t = \delta V_{bc} e^{-\lambda_{B3} r_{ij}} \quad (30)$$

Fig. 6 shows the influence of electrostatic shielding effect on the deformation bond energy calculated by **Eq. 25** and **Eq. 26**. **Eq. 25** represents the effect of deformation bond energy δV_{bc} on the ground state energy under different electrostatic shielding λ_{A1} . **Eq. 26** represents the effect of deformation bond energy δV_{bc} on density fluctuations under electrostatic shielding λ_{A2} . $t=b/z_x$ is overlapping integral. **Eq. 27** calculated the electrostatic shielding λ_{A3} values for MoS₂, MoSe₂ and MoTe₂, as is shown in the **Table 4**.

The potential energy surface and phase operator can be calculated as follows²⁶:

$$\begin{cases} V_i(\vec{r}_{ij}) = V_0(\vec{r}_{ij}) e^{-\lambda_i r_{ij}} \cos k_1 a \\ V_i(\vec{r}_{ij}) = V_0(\vec{r}_{ij}) e^{-\lambda_i r_{ij}} (\cos k_1 a + \cos k_2 a) \\ V_i(\vec{r}_{ij}) = V_0(\vec{r}_{ij}) e^{-\lambda_i r_{ij}} (\cos k_1 a + \cos k_2 a + \cos k_3 a) \end{cases} \quad (31)$$

Here, k_1 , k_2 and k_3 represent the components of \mathbf{k} in the x , y , and z directions, respectively. a is the lattice constant.

Tight-binding approximation of one-dimensional(1D) lattices:

$$\begin{cases} E(k) = \varepsilon_0 + 2t \cos k_1 a = \varepsilon_0 + 2\delta V_{bc} e^{-\lambda_i r_{ij}} \cos k_1 a \\ E_{band} = 2t \cos k_1 a = 2\delta V_{bc} e^{-\lambda_i r_{ij}} \cos k_1 a \end{cases} \quad (32)$$

Tight-binding approximation of 2D lattices:

$$\begin{cases} E(k) = \varepsilon_0 + 2t(\cos k_1 a + \cos k_2 a) = \varepsilon_0 + 2\delta V_{bc} e^{-\lambda_i r_{ij}} (\cos k_1 a + \cos k_2 a) \\ E_{band} = 2t(\cos k_1 a + \cos k_2 a) = 2\delta V_{bc} e^{-\lambda_i r_{ij}} (\cos k_1 a + \cos k_2 a) \end{cases} \quad (33)$$

Tight-binding approximation of three-dimensional(3D) lattices:

$$\begin{cases} E(k) = \varepsilon_0 + 2t(\cos k_1 a + \cos k_2 a + \cos k_3 a) = \varepsilon_0 + 2\delta V_{bc} e^{-\lambda_i r_{ij}} (\cos k_1 a + \cos k_2 a + \cos k_3 a) \\ E_{band} = 2t(\cos k_1 a + \cos k_2 a + \cos k_3 a) = 2\delta V_{bc} e^{-\lambda_i r_{ij}} (\cos k_1 a + \cos k_2 a + \cos k_3 a) \end{cases} \quad (34)$$

Using **Eq. 33** and **34** and overlaying integral $t=b/z$, we can calculate 2D and 3D energy band of MoS₂, MoSe₂ and MoTe₂, as is shown in the **Fig. 7**.

4. Conclusion

We computationally analyzed the electronic structure and bond properties of MoS₂, MoSe₂ and MoTe₂ materials. Our study found that electrostatic shielding by electron exchange is the main cause of density fluctuations. The density of the Green's function can be calculated from the energy shifts. These new methods and ideas can be applied to the study of atomic bonding, BE shift and electronic structure of materials in photoelectron spectroscopy measurement.

Table and Figure captions:

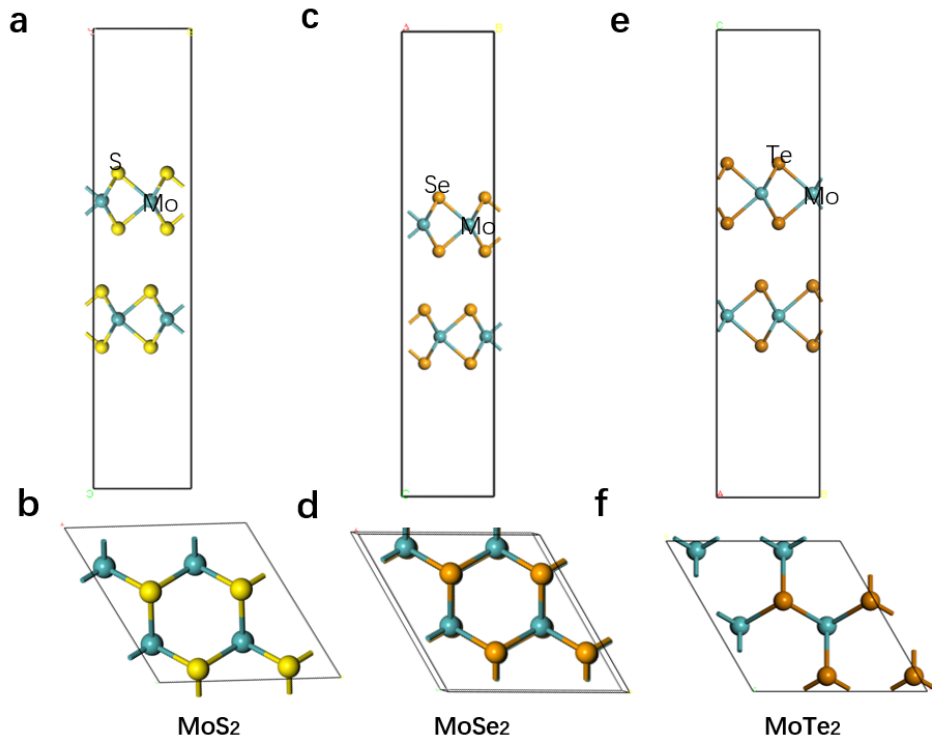
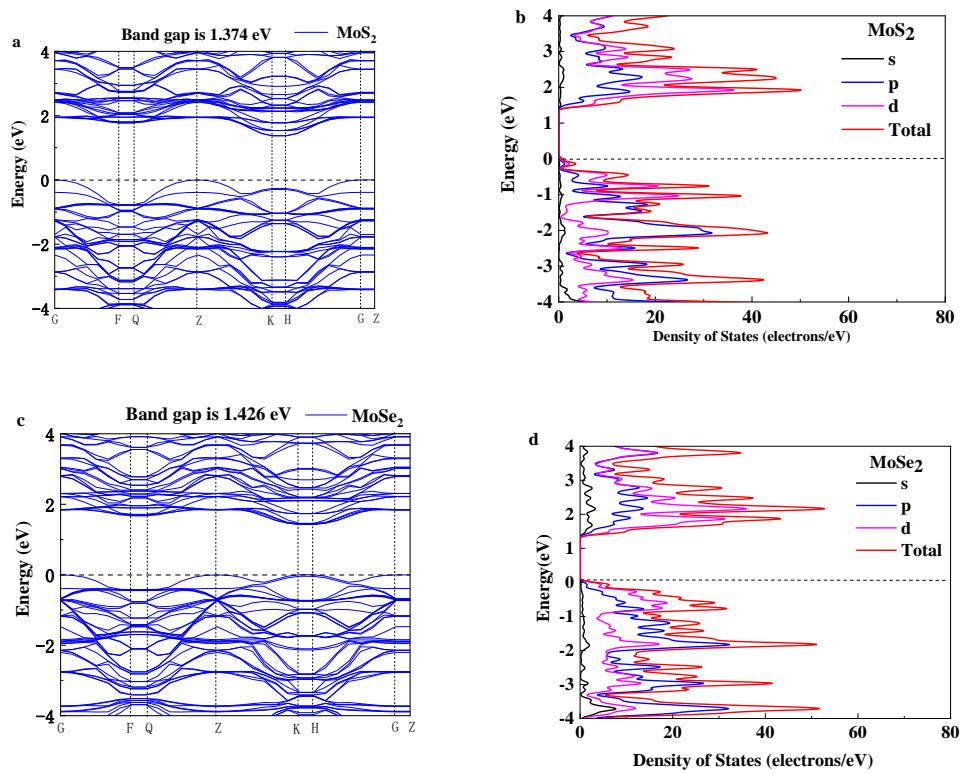


Fig. 1 Top (a) and side (b) views of the MoS₂. Top (c) and side (d) views of the MoSe₂. Top (e) and side (f) views of the MoTe₂.



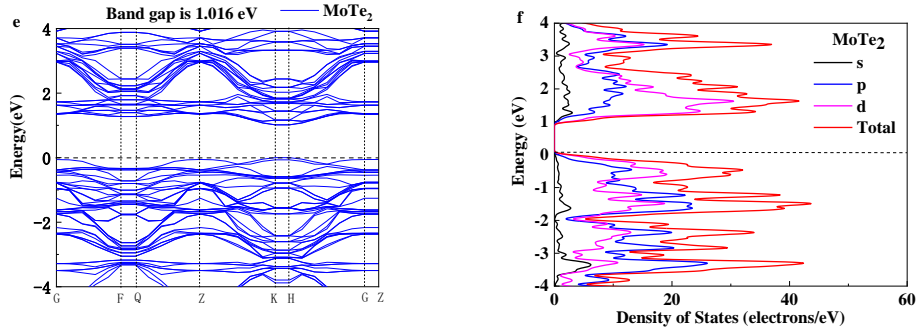


Fig. 2 Band structure of (a) MoS₂, (c) MoSe₂ and (e) MoTe₂. *s*-, *p*-, and *d*-orbital partial DOS of (a) MoS₂, (b) MoSe₂ and (e) MoTe₂.

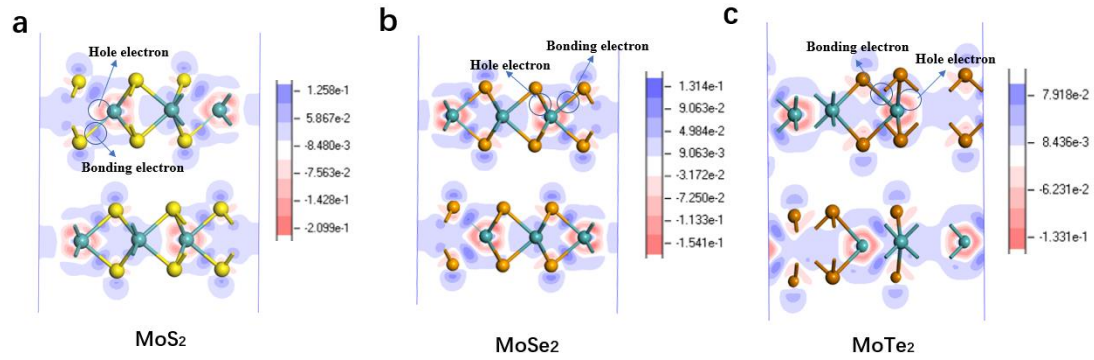


Fig. 3 Deformation charge density of (a) MoS₂, (b) MoSe₂ and (c) MoTe₂.

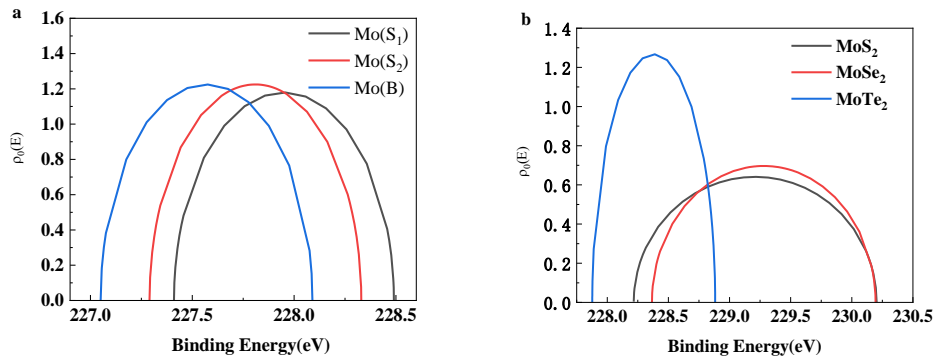


Fig. 4 Lattice density and BE shift of (a) Mo (100) surface²³ with three components representing the bulk B, S₂, and S₁ states. (b) MoS₂²⁷, MoSe₂²⁸, and MoTe₂²⁹.

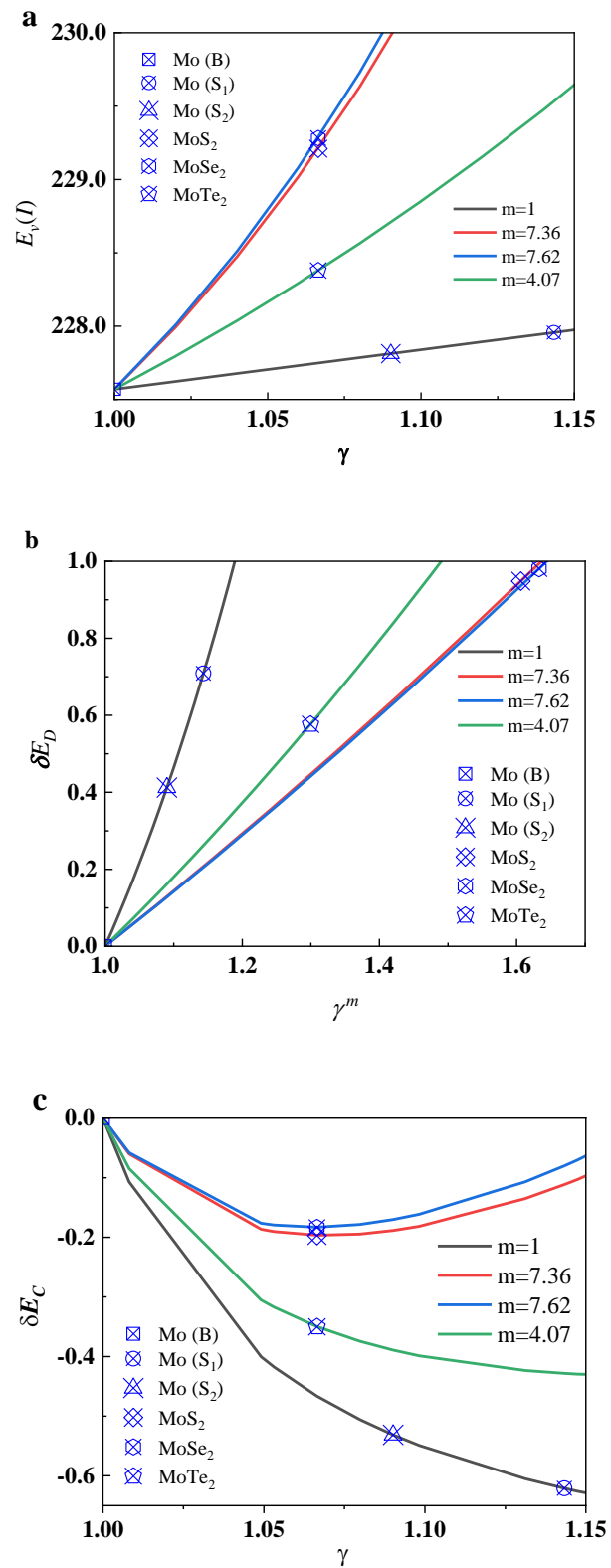


Fig. 5 BE ratio γ resolved (a) relative atomic cohesive energy δE_C (%), (b) relative bond energy density δE_D (%). m is an indicator for the bond nature. The related derived information is listed in

Table 4.

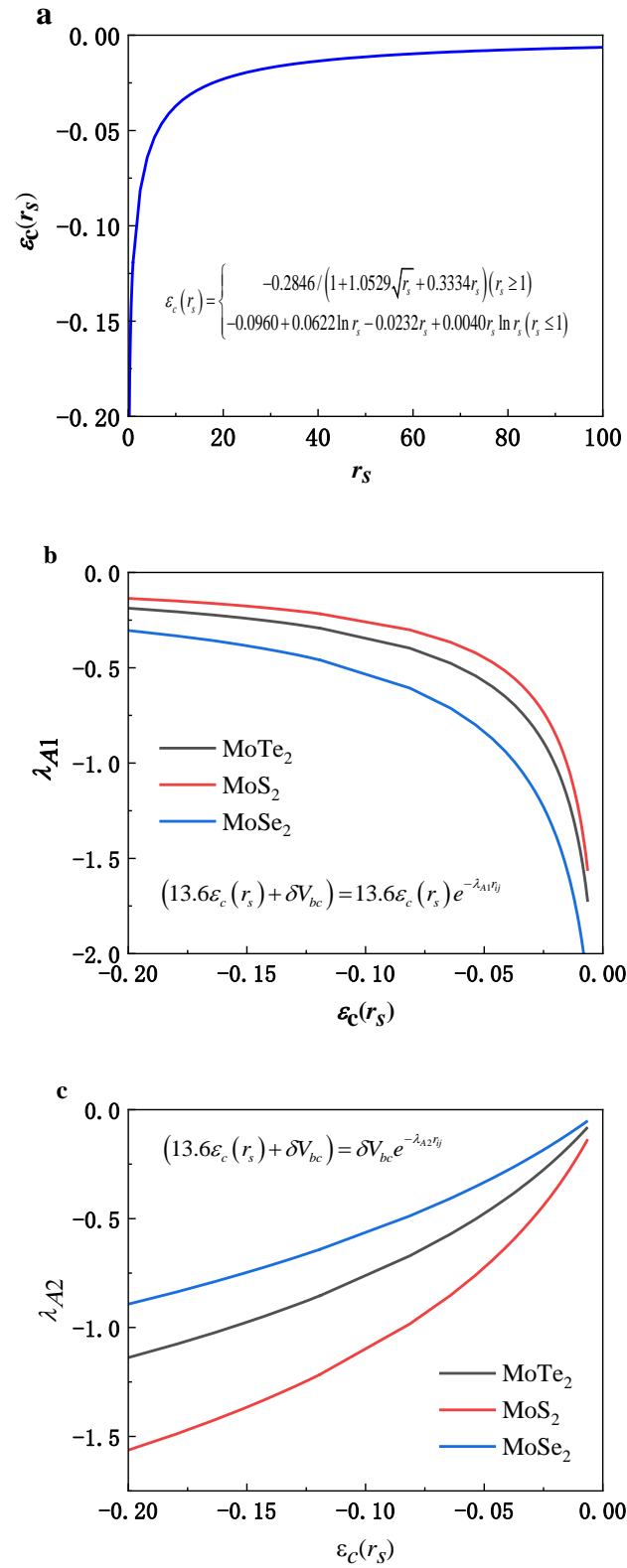


Fig. 6 Electrostatic shielding effect and energy scaling of MoS₂, MoSe₂ and MoTe₂

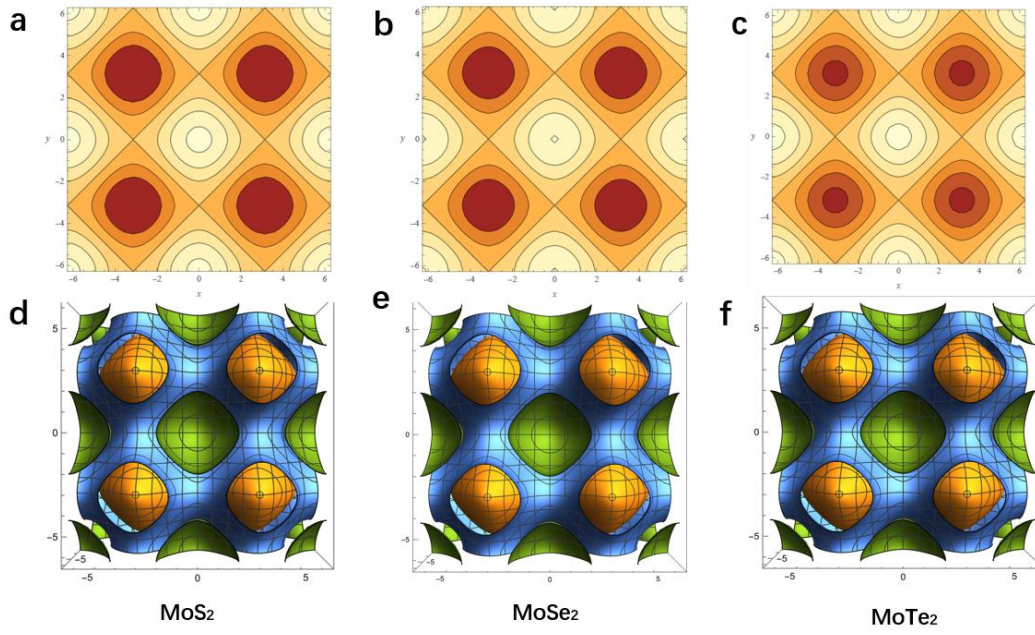


Fig. 7 2D (a) MoS₂, (b) MoSe₂, (c) MoTe₂, and 3D (a) MoS₂, (b) MoSe₂, (c) MoTe₂ energy band diagrams obtained by overlapping integral t .

Table 1 Lattice parameters of MoS₂, MoSe₂ and MoTe₂.

	Angle			Lattice parameters		
	α	β	γ	a (Å)	b (Å)	c (Å)
MoS ₂	90°	90°	120°	6.385	6.385	26.000
MoSe ₂	90°	90°	120°	7.123	7.123	28.000
MoTe ₂	90°	90°	120°	6.643	6.643	29.000

Table 2 Cut-off energies, band gap and k -points of MoS₂, MoSe₂ and MoTe₂.

Element	Cut-off energy	k -point	Band gap
MoS ₂	421.8 eV	8×8×1	1.374 eV
MoSe ₂	421.8 eV	8×8×1	1.426 eV
MoTe ₂	421.8 eV	8×8×1	1.023 eV

Table 3 Density of deformation charge $\delta\rho(\vec{r}_{ij})$, electrostatic shielding parameter λ_{A3} and the deformation bond energy $\delta V_{bc}(\vec{r}_{ij})$, as obtained by calculating the BBC model.

$$(\varepsilon_0 = 8.85 \times 10^{-12} \text{ C}^2 \text{ N}^{-1} \text{ m}^{-2}, e = 1.60 \times 10^{-19} \text{ C}, |\vec{r}_{ij}| \approx d_{ij} / 2)$$

	MoS ₂	MoSe ₂	MoTe ₂
r_{ij} (Å)	1.208	1.272	1.328
r_i (Å)	1.54 (Mo)	1.54 (Mo)	1.54 (Mo)
\vec{r}_j (Å)	1.05(S)	1.2(Se)	1.38(Te)
$\delta\rho^{\text{Hole-electron}}(\vec{r}_{ij}) \left(\frac{e}{\text{Å}^3} \right)$	-0.2099	-0.1541	-0.1331
$\delta\rho^{\text{Bonding-electron}}(\vec{r}_{ij}) \left(\frac{e}{\text{Å}^3} \right)$	0.1258	0.1314	0.07918
$\delta V_{bc}^{\text{bonding}}(\vec{r}_{ij})$ (eV)	-0.4851	-1.2864	-0.7692
λ_{A3}	0.9625	2.1516	1.1592

Table 4 Local bond strain ε_x (%), relative atomic cohesive energy δE_C (%), relative bond energy

density δE_D (%), indicator of bond nature m , BE ratio γ , overlapping integral t , atomic CN z_x ,

FWHM b and BE of Mo, MoS₂, MoSe₂ and MoTe₂.

		b	$E_V(I)$	z_x	t	γ^m	γ	m	ε_x (%)	δE_C (%)	δE_D (%)
Mo (100)	B	0.52	227.569	12.00	0.043	1.000	1	1	0	0	0
	S ₁	0.54	227.957	3.98	0.136	1.143	1.143	1	-12.53	-62.10	70.88
	S ₂	0.52	227.813	5.16	0.100	1.090	1.090	1	-8.27	-53.13	41.23
MoS ₂		0.99	229.210	6.00	0.165	1.606	1.066	7.36	-6.23	-19.69	94.84
MoSe ₂		0.91	229.282	6.00	0.152	1.633	1.066	7.62	-6.23	-18.36	98.07
MoTe ₂		0.50	228.380	6.00	0.083	1.30	1.066	4.07	-6.23	-35.02	57.65

References

- [1] H. Li, Q. Zhang, C. C. R. Yap, B. K. Tay, T. H. T. Edwin, A. Olivier, D. Baillargeat *Advanced Functional Materials*. **2012**, 22, 1385-1390.
- [2] Z. Wang, B. Mi *Environmental Science & Technology*. **2017**, 51, 8229-8244.
- [3] H. Li, J. Wu, Z. Yin, H. Zhang *Accounts of Chemical Research*. **2014**, 47, 1067-1075.
- [4] A. Splendiani, L. Sun, Y. Zhang, T. Li, J. Kim, C.-Y. Chim, G. Galli, F. Wang *Nano Letters*. **2010**, 10, 1271-1275.
- [5] R. Ganatra, Q. Zhang *ACS Nano*. **2014**, 8, 4074-4099.
- [6] D. Kong, H. Wang, J. J. Cha, M. Pasta, K. J. Koski, J. Yao, Y. Cui *Nano Letters*. **2013**, 13, 1341-1347.
- [7] X. Wang, Y. Gong, G. Shi, W. L. Chow, K. Keyshar, G. Ye, R. Vajtai, J. Lou, Z. Liu, E. Ringe, B. K. Tay, P. M. Ajayan *ACS Nano*. **2014**, 8, 5125-5131.
- [8] A. Eftekhari *Applied Materials Today*. **2017**, 8, 1-17.
- [9] C. Ruppert, B. Aslan, T. F. Heinz *Nano Letters*. **2014**, 14, 6231-6236.
- [10] S. Cho, S. Kim, J. H. Kim, J. Zhao, J. Seok, D. H. Keum, J. Baik, D.-H. Choe, K. J. Chang, K. Suenaga, S. W. Kim, Y. H. Lee, H. Yang *Science*. **2015**, 349, 625-628.
- [11] N. R. Pradhan, D. Rhodes, S. Feng, Y. Xin, S. Memaran, B.-H. Moon, H. Terrones, M. Terrones, L. Balicas *ACS Nano*. **2014**, 8, 5911-5920.
- [12] D. Voiry, M. Salehi, R. Silva, T. Fujita, M. Chen, T. Asefa, V. B. Shenoy, G. Eda, M. Chhowalla *Nano Letters*. **2013**, 13, 6222-6227.
- [13] S. Larentis, B. Fallahazad, E. Tutuc *Applied Physics Letters*. **2012**, 101.
- [14] X. Luo, F. C. Chen, J. L. Zhang, Q. L. Pei, G. T. Lin, W. J. Lu, Y. Y. Han, C. Y. Xi, W. H. Song, Y. P. Sun *Applied Physics Letters*. **2016**, 109.
- [15] K. Deng, G. Wan, P. Deng, K. Zhang, S. Ding, E. Wang, M. Yan, H. Huang, H. Zhang, Z. Xu, J. Denlinger, A. Fedorov, H. Yang, W. Duan, H. Yao, Y. Wu, S. Fan, H. Zhang, X. Chen, S. Zhou *Nature Physics*. **2016**, 12, 1105-1110.
- [16] H. Qiu, H. Li, J. Wang, Y. Zhu, M. Bo *physica status solidi (RRL)–Rapid Research Letters*. **2022**, 16, 2100444.
- [17] J. P. Perdew, K. Burke, M. Ernzerhof *Physical review letters*. **1996**, 77, 3865.
- [18] M. Gell-Mann, K. A. Brueckner *Physical Review*. **1957**, 106, 364-368.
- [19] J. P. Perdew, A. Zunger *Physical Review B*. **1981**, 23, 5048-5079.
- [20] W. A. Schwalm, M. K. Schwalm *Physical Review B*. **1988**, 37, 9524-9542.
- [21] C. Q. Sun *Progress in Solid State Chemistry*. **2007**, 35, 1-159.
- [22] M. Bo, Y. Guo, X. Yang, J. He, Y. Liu, C. Peng, Y. Huang, C. Q. Sun *Chemical Physics Letters*. **2016**, 657, 177-183.
- [23] W. Zhou, M. Bo, Y. Wang, Y. Huang, C. Li, C. Q. Sun *RSC Advances*. **2015**, 5, 29663-29668.
- [24] D. M. Ceperley, B. J. Alder *Physical Review Letters*. **1980**, 45, 566-569.
- [25] R. Resta *Physical Review B*. **1977**, 16, 2717-2722.
- [26] Z. Wang, Y. Huang, F. Li, Y. Chuang, Z. Huang, M. Bo *Chemical Physics Letters*. **2022**, 808, 140124.
- [27] M. A. Baker, R. Gilmore, C. Lenardi, W. Gissler *Applied Surface Science*. **1999**, 150, 255-262.

- [28] L. Wang, J. Zhao, X. Tang, S. Kuang, L. Qin, H. Lin, Q. Li *Surfaces and Interfaces*. **2023**, *39*, 102956.
- [29] K. Ueno, K. Fukushima *Applied Physics Express*. **2015**, *8*, 095201.